

1. INTRODUCTION

It is well known from numerical simulations that sheared flows with critical levels may lead to resonance with high drag regimes. These resonant flows have been studied mostly in highly nonlinear situations (Bacmeister and Pierrehumbert 1988) and the enhancement of the drag has been attributed to nonlinear processes, such as wave breaking. Existing theories explain the resonant drag enhancement and the associated downslope windstorms either using a hydraulic analogy (Smith 1985) or postulating the reflection of the internal gravity waves at pre-existent or wave induced critical levels (Clark and Peltier 1984). However, 2D and 3D numerical results have shown a significant difference in the vertical distribution of resonant critical levels (Miranda and Valente 1997). There is also some controversy regarding the role played by the Richardson number at the critical level in determining high drag states (Scinocca and Peltier 1991). This study is an attempt to shed some light on these issues using linear theory - recent studies on wave ducting (Wang and Lin 1999) suggest that linear theory may provide some useful insights into the drag amplification mechanism.

2. THEORETICAL MODEL

The drag associated with resonant flow past 2D and 3D topographic obstacles is studied analytically using a simple linear hydrostatic model. The wind profile is assumed to have the form

$$U = \begin{cases} U_0 & \text{if } z \leq z_1 \\ U_0 \left(\frac{z_c - z}{z_c - z_1} \right) & \text{if } z > z_1 \end{cases} \quad (1)$$

$V=0,$

where U_0 is the surface wind, z_1 is the level where the wind velocity changes from constant to backward linear and z_c is the critical level (where $U=0$). This flow is similar to that used by Miranda and Valente (1997) and Wang and Lin (1999) up to a certain height above the critical level. Here, sufficiently high Richardson numbers are considered in the shear region, so that the wave energy is essentially absorbed at the critical level and what happens above is approximately irrelevant (Grubišić and Smolarkiewicz 1997). The Taylor-Goldstein equation,

$$\hat{w}'' + \left(\frac{N^2 k_{12}^2}{(Uk_1 + Vk_2)^2} - \frac{U''k_1 + V''k_2}{Uk_1 + Vk_2} \right) \hat{w} = 0, \quad (2)$$

determines the solution for the Fourier transform of the vertical velocity perturbation induced by the mountain, \hat{w} , for an internal gravity wave of wavenumber (k_1, k_2) (with $k_{12} = (k_1^2 + k_2^2)^{1/2}$) and a background flow with Brunt-Väisälä frequency N and wind velocity $(U(z), V(z))$. This equation is subject to the boundary condition that the flow follows the topography at the surface,

$$\hat{w}(z=0) = i(U_0 k_1 + V_0 k_2) \hat{\eta}, \quad (3)$$

where (U_0, V_0) is the background wind at the surface and $\hat{\eta}$ is the Fourier transform of the terrain elevation. Additionally, it is required that the wave energy flows upwards in the upper layer ($z > z_1$), and that both the vertical velocity and the pressure be continuous at $z = z_1$. In practice, these two latter conditions are imposed on \hat{w} and on the Fourier transform of the pressure,

$$\hat{p} = i \frac{\rho_0}{k_{12}^2} [(U'k_1 + V'k_2) \hat{w} - (Uk_1 + Vk_2) \hat{w}'], \quad (4)$$

where ρ_0 is a reference density (assumed constant).

The drag force associated with this flow can be calculated, for an isolated 3D mountain, from

$$(D_x, D_y) = 4\pi^2 i \int_{-\infty-\infty}^{+\infty+\infty} \int_{-\infty-\infty}^{+\infty+\infty} (k_1, k_2) \hat{p}^*(z=0) \hat{\eta} dk_1 dk_2, \quad (5)$$

while for an infinite, 2D ridge, the corresponding drag per unit spanwise length is

$$D_x = 2\pi i \int_{-\infty}^{+\infty} k_1 \hat{p}^*(z=0) \hat{\eta} dk_1, \quad (6)$$

where the asterisk denotes complex conjugate and the ridge is assumed to be along the y direction.

Once (2) is solved and the resulting expression for \hat{p} obtained from (4) is introduced into (5) or (6), it becomes clear that the drag divided by its value for a constant wind profile, D_0 , does not depend on the detailed shape of the orography as long as this is axisymmetric (in (5)) or 2D (in (6)) (cf. Teixeira et al. 2004). The final expression for the normalized drag on an axisymmetric mountain is thus

$$\frac{D}{D_0} = \frac{1}{\pi} \int_0^{2\pi} \frac{\cos^2 \theta \left(1 - \frac{1}{4} Ri^{-1} \cos^2 \theta \right)^{1/2}}{1 - \frac{1}{2} Ri^{-1/2} \cos \theta \sin \left(\frac{2N}{U_0 \cos \theta} z_1 \right)} d\theta, \quad (7)$$

and the normalized drag on a 2D ridge is

$$\frac{D}{D_0} = \frac{\left(1 - \frac{1}{4} Ri^{-1} \right)^{1/2}}{1 - \frac{1}{2} Ri^{-1/2} \sin \left(\frac{2N}{U_0} z_1 \right)}. \quad (8)$$

* Corresponding author address: Miguel A. C. Teixeira, Centro de Geofísica da Universidade de Lisboa, Edifício C8, Campo Grande, 1749-016 Lisbon, Portugal

In (7) and (8), D denotes D_x , since that is the only non-zero drag component for the flow (1), and $Ri = N^2(z_c - z_1)^2 / U_0^2$ is the Richardson number in the shear layer.

3. RESULTS

3.1. Drag for a 2D ridge

Equation (8) shows that the normalized drag in flow over a 2D ridge is given by a closed analytical expression, which is easy to interpret. When $z_1=0$, the drag reduces to that calculated by Smith (1986) (his eq. (3.17)), decreasing from 1 to 0 as Ri goes from $+\infty$ to $1/4$. When $z_1>0$, the drag oscillates as z_1 increases, and the period of the oscillation (in terms of z_1) is of half the hydrostatic vertical wavelength, U_0/N . This oscillation is modulated by Ri , so that its amplitude tends to zero when $Ri \rightarrow \infty$ and to infinity when $Ri=1/4$.

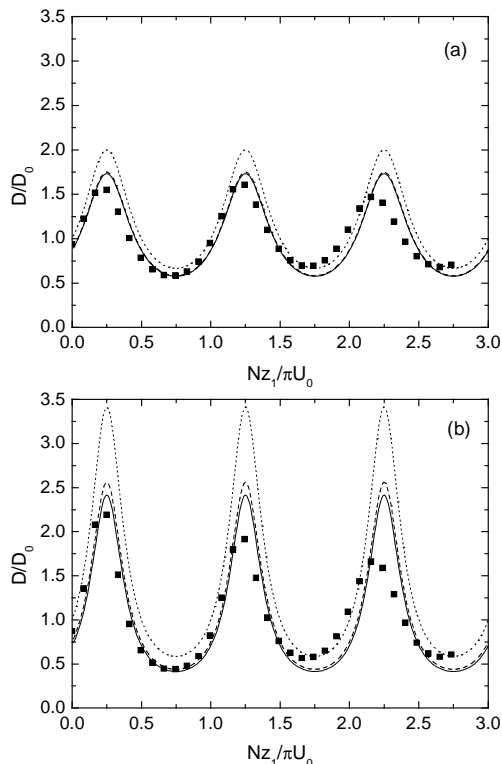


Fig. 1. Normalized drag as a function of normalized height. Solid line: eq. (8), dotted line: 1st order WKB, dashed line 2nd order WKB, symbols: NH3D. (a) $Ri=1$, (b) $Ri=0.5$.

Fig. 1 compares the variation of the normalized drag with $Nz_1/\pi U_0$ for $Ri=1$ and $Ri=0.5$ predicted by (8) and results from a non-hydrostatic mesoscale numerical model (NH3D). For the conditions considered in the runs, which were very approximately linear and hydrostatic, the agreement is fairly good. While (8) predicts that the amplitude of the peaks is constant, in the numerical simulations this amplitude becomes smaller for the largest $Nz_1/\pi U_0$ considered. This is

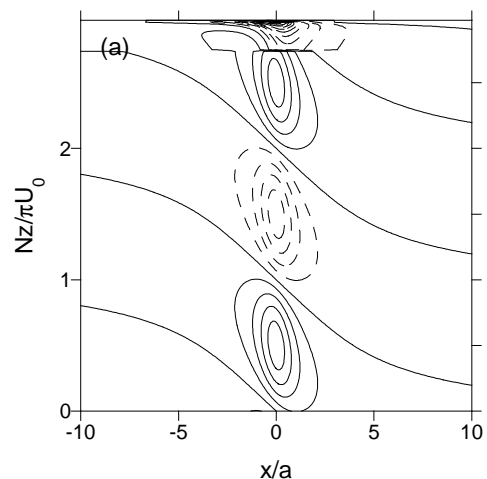
probably a spurious effect due to the momentum flux profile not having attained a steady state in the runs at high levels. Also shown as the dotted and dashed lines are the 1st and 2nd order WKB solutions calculated by the method described in Teixeira et al. (2004). These solutions assume that, in the region $z>z_1$, the wind varies relatively slowly (this is manifestly not true near z_c). As in the study of Teixeira et al. (2004), it is necessary to extend the WKB solution to 2nd order if the numerical results are to be predicted accurately. The 1st order solution overestimates the data, slightly for $Ri=1$ and considerably for $Ri=0.5$. However, the 2nd order solution is quite accurate even for $Ri=0.5$ and despite the existence of the critical level.

These results show that the process responsible for amplifying the drag for very gentle mountains is indeed linear resonance. This case is of limited relevance, since the absolute values of the drag in linear flow are always very small. Most mountains generate nonlinear waves, where the drag enhancement is considerably larger, and the spacing between maxima becomes of one vertical wavelength. Nevertheless, the present calculations suggest that the key height in the drag amplification process is z_1 instead of z_c (as proposed by Wang and Lin 1999) and that Ri is an important parameter of the flow, modulating the drag amplification.

3.2. Flow structure

At z_1 , the mountain wave is reflected partially, leading to the reinforcement or weakening of the pressure perturbation at the surface. This process is understood better by analyzing the vertical structure of the flow.

Fig. 2. shows vertical cross sections of the streamwise velocity perturbation, calculated from the analytical model for a bell-shaped ridge of width a , at $Ri=0.5$, which in the region $z<z_1$ is equal in value but of opposite sign to the pressure perturbation. The off-resonance case (a) corresponds to the third trough in fig.1 and the on-resonance case (b) to the fourth peak (outside the graph). Although the amount of reflection at z_1 is the same in the two cases, it is clear that this causes a cancellation of the wave perturbation in the first case and a reinforcement in the second.



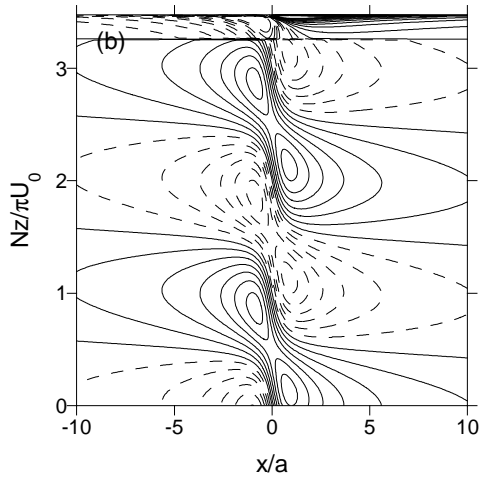


Fig. 2. Vertical cross-section of the normalized streamwise velocity perturbation. Solid contours: positive values, dashed contours: negative values. (a) $Nz_1/\pi U_0=2.75$, (b) $Nz_1/\pi U_0=3.25$.

Not only is the perturbation stronger in the on-resonance case, but it is also more anti-symmetric relative to the ridge (centered at $x/a=0$), having a phase relation that favors drag enhancement.

These aspects are confirmed by fig. 3, where the isentropes of these two flows (corresponding to streamlines) are presented. The amplitude of the perturbations was exaggerated by considering a dimensionless mountain height of 0.5 (for which linear theory would not be valid). It is visible that, in the off-resonance case (a), the amplitude of the waves is relatively small and near the surface the isentropes are almost symmetric relative to the ridge, while in the on-resonance case (b), the isentropes are strongly perturbed throughout the flow and display a marked asymmetry. They are much closer to each other on the downwind side of the mountain than on the upwind side, which is consistent with a relatively high drag. Although not as pronounced as in nonlinear cases, the flow structure in fig. 3(b) clearly resembles the severe drag configurations of Bacmeister and Pierrehumbert (1988).

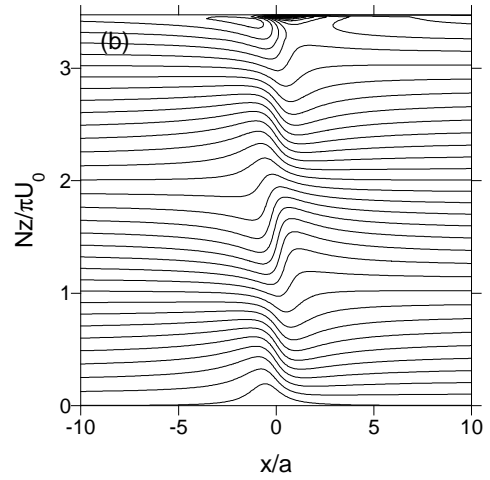
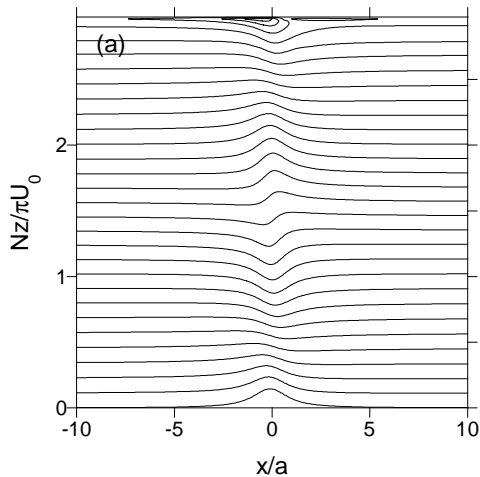
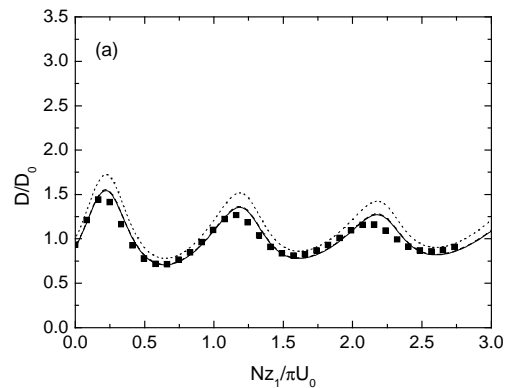


Fig. 3. Vertical cross-section of the isentropes for a ridge of dimensionless height 0.5. Contour spacing: 1K. (a) $Nz_1/\pi U_0=2.75$, (b) $Nz_1/\pi U_0=3.25$.

3.3. Drag for an axisymmetric mountain

Equation (7) suggests that the drag behavior for flow over an axisymmetric mountain is broadly similar to that in flow over a ridge. The differences are due to the dispersiveness of the waves in the former case. Because of this, when $z_1=0$, although the drag decreases as Ri decreases, it does not reach zero for $Ri=1/4$ (cf. Grubišić and Smolarkiewicz 1997). On the other hand, when $z_1>0$, although the amplitude of the drag modulation increases as Ri decreases, it never becomes infinite.

Fig. 4 displays the normalized drag as a function of $Nz_1/\pi U_0$ for $Ri=1$ and $Ri=0.5$. It can be seen that the amplitude of the drag modulation is smaller than in the 2D case, and tends to become even smaller for large $Nz_1/\pi U_0$. This effect is now physically real and due to wave dispersion. The agreement with data from the numerical model NH3D is once again satisfactory for approximately linear and hydrostatic conditions, although there is still a slight spurious damping of the oscillations in the runs for large $Nz_1/\pi U_0$ due to the reasons pointed out in section 3.1. The 2nd order WKB solution is also here considerably more accurate than the 1st order WKB solution.



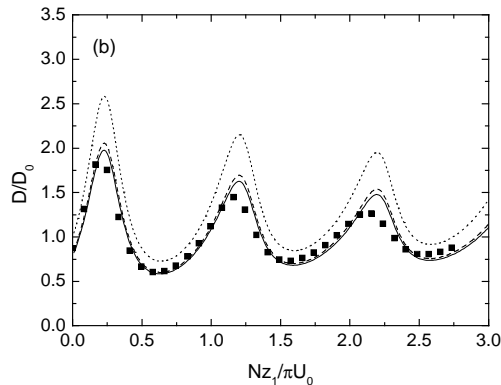


Fig. 4. Normalized drag as a function of normalized height. Solid line: eq. (7), dotted line: 1st order WKB, dashed line: 2nd order WKB, symbols: NH3D. (a) $Ri=1$, (b) $Ri=0.5$.

3.4 Nonlinear effects

For mountains with dimensionless heights of order one, the predictions of linear theory are of limited interest. A drastic change in behavior is observed for flow past an infinite ridge, with much larger drag amplification, disappearance of the second maximum in fig. 1 (Clark and Peltier 1984) and the existence of resonance shift (Smith 1985), whereby the drag maxima, as represented in fig.1, are displaced to the right. However the behavior of the drag does not seem to change very much in the case of an axisymmetric mountain, as shown by Miranda and Valente (1997).

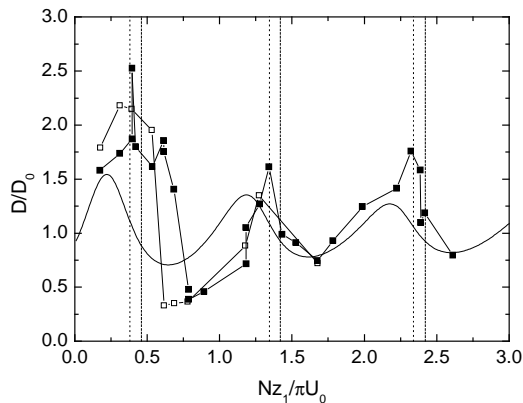


Fig. 5. Normalized drag as a function of normalized height for $Ri=1$. Solid line: eq. (7), open squares: NH3D, dimensionless height 0.5, filled squares: NH3D, dimensionless height 0.75 (Miranda & Valente 1997).

In fig. 5 it can be seen that, although for the strongly nonlinear flows corresponding to the runs of the NH3D model, the drag is considerably underestimated by (7), especially the first maximum, the general tendency of the maxima to decrease in magnitude as $Nz_1/\pi U_0$ increases is captured. The dashed and dotted vertical lines correspond to the sum of the dimensionless heights where (7) predicts the maxima to occur and the dimensionless mountain heights 0.5 and 0.75, respectively. Since the flow is displaced upward by

the mountain, one would expect that the maxima in the numerical data would fall between the maxima of the solid line and the vertical lines - which indeed happens. This supports, on the one hand, the importance of z_1 as a key height of this problem and, on the other, the insignificance of resonance shift in the 3D case. This is in contrast with what happens in flow over a 2D ridge, where a similar correction was found to be insufficient to explain the location of the drag maxima.

In fig. 5, there is also a visible sharpening of the drag maxima and a slight lowering of the second maximum, which might be an incipient manifestation of the phenomenon that suppresses this maximum in the 2D case.

4. DISCUSSION

The present results show that high-drag states exist even in flow over very gentle topography, and help to clarify the dynamics of the drag modulation process (in particular emphasizing the importance of the level where the vertical wind gradient is discontinuous). Although a hyperbolic-tangent velocity profile (used in many studies of this problem) has no discontinuity in its gradient, one can think of the zone where this profile has a maximum in negative curvature as being a sort of attenuated discontinuity, with an essentially equivalent reflecting effect. The present model also shows how the amplitude of the drag modulation depends crucially on the Richardson number. It would be interesting to check whether this also happens in strongly nonlinear flows.

5. REFERENCES

- Bacmeister, J. T. and Pierrehumbert, R. T., 1988: On the high-drag states of nonlinear stratified flow over an obstacle. *J. Atmos. Sci.*, **45**, 63-80.
- Clark, T. L. and Peltier, W. R., 1984: Critical level reflection and resonant growth of nonlinear mountain waves. *J. Atmos. Sci.*, **41**, 3122-3134.
- Grubišić, V. and Smolarkiewicz, P. K., 1997: The effect of critical levels on 3D orographic flows: linear regime. *J. Atmos. Sci.*, **54**, 1943-1960.
- Miranda, P. M. A. and Valente, M. A., 1997: Critical level resonance in three-dimensional flow past isolated mountains. *J. Atmos. Sci.*, **54**, 1574-1588.
- Scinocca, J. F. and Peltier, W. R., 1991: On the Richardson number dependence of nonlinear critical-layer flow over localized topography. *J. Atmos. Sci.*, **48**, 1560-1571.
- Smith, R. B., 1985: On severe downslope windstorms. *J. Atmos. Sci.*, **42**, 2597-2603.
- Smith, R. B., 1986: Further development of a theory of lee cyclogenesis. *J. Atmos. Sci.*, **43**, 1582-1602.
- Teixeira, M. A. C., Miranda, P. M. A. and Valente, M. A., 2004: An analytical model of mountain wave drag for wind profiles with shear and curvature. *J. Atmos. Sci.*, **61**, 1040-1054.
- Wang, T.-A. and Lin, Y.-L., 1999: Wave ducting in a stratified shear flow over a two-dimensional mountain. Part I: General linear criteria. *J. Atmos. Sci.*, **56**, 412-436.